

Behavior of numerical error in pore-scale lattice Boltzmann simulations with simple bounce-back rule: Analysis and highly-accurate extrapolationSiarhei Khirevich^{1, a)} and Tadeusz W. Patzek¹*Ali I. Al-Naimi Petroleum Engineering Research Center,
King Abdullah University of Science and Technology, Thuwal,
Saudi Arabia*

(Dated: 14 September 2018)

We perform the viscosity-independent Stokes flow simulations in regular sphere packings using the two-relaxation-times (TRT) lattice Boltzmann Method (LBM) with the simple bounce-back rule (BB). Our special discretization procedure reduces the scatter in integral quantities, such as drag force, and quantifies the solution convergence error. We assume transition to linear (-1) convergence rate for different sets of TRT parameters and use this assumption to provide a simple extrapolation scheme. After establishing the accurate reference values of drag for a wide range of porosities, 0.26–0.78, we show a ten-fold decrease in drag error using the suggested extrapolations. This error decrease allows the simple LBM/BB scheme reach accuracy of the high-order interpolated boundary schemes. The suggested extrapolation approach is straightforward to apply in porous media, whose pore space can be discretized at several resolutions.

^{a)}Electronic mail: siarhei.khirevich@kaust.edu.sa

I. INTRODUCTION

Over the last few decades, the lattice-Boltzmann method (LBM) has been widely used to calculate the single- and two-phase flow of incompressible and immiscible fluids^{1–4} in the morphologically and topologically complex pore space of clastics and carbonates. In addition to accuracy of LBM discretizations, the pore space itself can never be described accurately^{5–8} by the finite resolution reconstructions. This confluence of difficulties with numerical and imaging approximations leads to an interesting question: What fraction of computational inaccuracy in flow and transport calculations is caused by the pore space discretization and how much of it originates in the flow calculations with LBM? In this paper, we try to provide quantitative answers pertinent to the latter.

By extending an earlier result⁹, we derive a simple method of increasing accuracy of one of the simplest LBM implementations. The key reasons for LBM’s popularity in calculating incompressible flows in porous media have been (i) relative simplicity of its implementation and (ii) acceptable accuracy while using regular meshes to resolve complex solid boundaries. Kinetic origin of LBM assumes the use of collision rules for evolving its particles; one of the popular set of rules is the Bhatnagar–Gross–Krook collision operator (BGK)^{10–12}. Despite its popularity, BGK is well known for the dependency of permeability (or drag force) on the viscosity of simulated fluid^{13–15}. Reformulation of the matrix–collision model¹⁶ resulted in the multiple-relaxation-times collision operator (MRT) with several adjustable parameters. A reduced version of MRT developed later, the two-relaxation-times (TRT) collision operator^{17,18}, is well suited for solving advection–diffusion problems and performing Navier–Stokes simulations¹⁹.

Until now, choices of relaxation parameters in the TRT and MRT schemes have remained an open question¹⁹. Analytical evaluation of the TRT operator demonstrated that a specific combination Λ (known as “magic number”¹⁹) of its two relaxation parameters controls the viscosity-independent steady solutions in any geometry. In Poiseuille flow simulations using bounce-back rule (see below) with walls located midway the intersected links, $\Lambda = 3/16$ and $\Lambda = 3/8$ provide exact velocity profile in a channel oriented horizontally or diagonally with respect to the lattice¹³; the value of $\Lambda = 1/8$ gives the exact average flow rate through the channel. For flows in complex geometries, these values of Λ provide solutions of acceptable accuracy for medium resolutions and above, e.g.⁹. It was established^{9,20} that values of Λ

outside of the interval $[1/8, 3/8]$ can change significantly the simulated flow field in porous media. Therefore, the parameter Λ can be a powerful tool that controls simulation accuracy.

Regular sphere packings represent a good underlying geometry to assess accuracy of LBM simulations in porous media: they are simple enough to be approached (semi-)analytically, yielding a number of independently-obtained solutions^{21–23}. At the same time, the converging/diverging flow in packings makes this geometry clearly more complex than flow between two parallel plates or through a square duct. It is also worth mentioning that sphere packings represent real systems in chromatography²⁴ and chemical engineering²⁵.

Popularity of the lattice Boltzmann method^{26–29} as a flow solver can be attributed to its acceptable accuracy while using the bounce-back boundary condition (BB)^{9,30}, for which the lattice populations facing a solid voxel are reflected back from it. Simplicity, locality, and robustness of BB made it attractive among other boundary rules. However, detailed analysis of numerical LBM/BB solutions did not prove their convergence to accurate solutions in complex geometries^{14,15,30,31}, despite theoretical analysis suggesting that this must be the case³². Inaccuracies of LBM/BB simulations have led to various improvements, such as effective hydrodynamic radius³³ or extrapolation of simulation results towards the infinitely high discretization resolution³⁴.

Validation of flow simulations in regular packings against independent solutions is often difficult because of the significant scatter of LBM/BB results. This scatter leads to statements about the different convergence behavior of random and regular packings or to questioning convergence of LBM/BB to the true solution³⁰. In addition, the ubiquitous use of the -2 convergence rate for extrapolation^{34,35}, complicates understanding of convergence of LBM/BB in complex geometries.

The interpolated or multi-reflection boundary condition (IMR) algorithms solve for the intersections of analytical boundary and LBM lattice links. This feature makes LBM/IMR significantly more accurate than LBM/BB. Solutions obtained with the IMR boundary conditions demonstrate much weaker dependency on Λ compared with the bounce-back rule^{9,15}. Despite improved accuracy and convergence rates^{9,14,30,31,36}, implementation of LBM/IMR requires additional programming to modify flow solver³⁰ for each type of considered geometries, e.g., for sphere packings vs. fractures. It has been reported that i) the interpolated boundary conditions do not always conserve the total fluid mass^{14,36}, and ii) some of the advanced boundary condition schemes require more-than-first lattice neighbor, thus diminishing LBM

locality and degrading scaling efficiency of parallel LBM implementations³⁷.

In this work, we focus only on the bounce-back boundary condition and extend the results of an earlier study by Khirevich et al.⁹. Using the previously introduced discretization procedure, we reduce significantly the scatter of the solutions. With less scatter, we analyze the behavior of numerical error and observe convergence to the -1 rate for a wide range of TRT parameters. We suggest a simple extrapolation approach and demonstrate a ten-fold reduction of relative error in integral quantities such as permeability or drag.

II. SIMULATION APPROACH

We solve the Stokes problem in a periodic domain for the momentum \vec{j} of an incompressible fluid driven by a body force \vec{B} :

$$\mu\Delta\vec{j} + \vec{B} = 0, \quad (1a)$$

$$\vec{j} = \rho_0\vec{u}, \quad (1b)$$

where μ is the kinematic viscosity, ρ_0 is the fluid density, and \vec{u} is the fluid velocity. The Stokes flow regime is typical of the porous media in which inertia is dominated by viscosity.

The average normalized drag force F_d exerted on a single sphere (cf. van der Hoef et al.³⁴) is:

$$F_d = \frac{d_{\text{sp}}^2}{18(1 - \varepsilon)k}, \quad (2)$$

where d_{sp} is the sphere diameter, ε is the porosity, and k is the permeability. Later in this work, we consider d_{sp} to be expressed in lattice units and ε is taken as the ratio of fluid voxels to the total number of voxels. Permeability is calculated using Darcy's law:

$$k \equiv k_x = \frac{\mu\varepsilon j_x}{B_x} \quad (3)$$

In the equation above, we assume that the simulation domain is isotropic and the permeability tensor is a scalar.

A. Two-relaxation-times lattice Boltzmann scheme

To solve eqs. (1), we employ the two-relaxation-times lattice Boltzmann method^{17-20,38}. LBM simulates behavior of fictitious particles that reside on a discrete cubic lattice and

evolve at discrete time steps t . Each lattice site \vec{x} is occupied by Q ($= 19$ in this study) particle populations f_q , consisting of one immobile particle and $Q_m = Q - 1$ mobile ones. The lattice sites are interconnected by Q_m velocity vectors c_q . Using a symmetry argument, we group the velocity vectors into “links” $\{c_q, c_{\bar{q}}\}$ such that $c_{\bar{q}} = -c_q$. In each time step, the particles propagate along the lattice vectors and collide according to the following rule:

$$f_q(\vec{x} + \vec{c}_q, t + 1) = \tilde{f}_q(\vec{x}, t), \quad (4)$$

$$\tilde{f}_q(\vec{x}, t) = [f_q - s^+(f_q^+ - e_q^+) - s^-(f_q^- - e_q^-) + S_q^+ + S_q^-](\vec{x}, t), \quad (5)$$

$$q = 0, \dots, Q_m/2$$

$$\tilde{f}_{\bar{q}}(\vec{x}, t) = [f_{\bar{q}} - s^+(f_q^+ - e_q^+) + s^-(f_q^- - e_q^-) + S_q^+ - S_q^-](\vec{x}, t), \quad (6)$$

$$q = 1, \dots, Q_m/2$$

where $f_q^\pm = (f_q \pm f_{\bar{q}})/2$, tilde \sim denotes the post-collision state, and the equilibrium functions e_0 and e_q^\pm are calculated using the local mass ρ and momentum \vec{J} as

$$\rho = f_0 + 2 \sum_{q=1}^{Q_m/2} f_q^+, \quad \vec{j} = \vec{J} + \frac{1}{2}\vec{B}, \quad \vec{J} = 2 \sum_{q=1}^{Q_m/2} f_q^- \vec{c}_q, \quad (7)$$

$$e_q^+ = c_s^2 t_q \rho, \quad e_q^- = t_q (\vec{J} \cdot \vec{c}_q), \quad \text{and} \quad e_0 = \rho - 2 \sum_{q=1}^{Q_m/2} e_q^+. \quad (8)$$

Here c_s^2 denotes the speed of sound and t_q are the isotropic weights of $1/6$ and $1/12$ for the 6 “horizontal” and 12 “diagonal” lattice vectors, respectively. The quantity S^+ denotes the mass sources, here equal 0, while S^- is the body force driving the fluid:

$$S_q^- = t_q \rho_0 (\vec{B} \cdot \vec{c}_q). \quad (9)$$

The relaxation parameters s^\pm are limited to the $]0, 2[$ interval, and a particular value of s^+ defines the fluid viscosity as $\nu = (1/s^+ - 1/2)/3$, while the parameter s^- is free-tunable. Let us introduce the following ratio between s^+ and s^- :

$$\Lambda = (1/s^+ - 1/2)(1/s^- - 1/2), \quad (10)$$

which is also known as “magic number”¹⁹. The ratio Λ controls the location of zero-velocity boundary within the simulated geometry (for instance, see Figure 1 in⁹), and therefore defines the stationary flow field up to machine accuracy for any combination of the two relaxation

parameters s^\pm as well as body force values^{17,19}. In other words, Λ directly controls the output integral quantities such as total momentum, permeability, and drag force.

All the results in this paper can be reproduced using the BGK collision operator, keeping in mind the following relations between Λ , fluid viscosity, and the single relaxation parameter τ of the BGK model:

$$\Lambda = 9\nu^2, \quad (11)$$

$$\Lambda = \left(\tau - \frac{1}{2}\right)^2. \quad (12)$$

In the BGK collision operator, the fluid viscosity is controlled solely by τ . Therefore, selecting τ at a value that matches the TRT solution with a given Λ fixes the corresponding value of ν . As a result, a non-optimal combination of the viscosity ν , desired accuracy, and simulation geometry *may* negatively impact execution time to reach steady state (see Figure 5 in²⁰ and Figure 7 in⁹).

B. Steady-state solution

Evolution of LBM solution in pore-scale simulations typically demonstrates oscillatory behavior (for example, see Figure 7 in⁹), which mainly depends on the lattice viscosity as well as on the geometry of the simulation domain. In this work, our goal is to estimate integral quantities, such as drag force, and therefore we use the following termination criterion:

$$M_T^i = \left| \frac{j_x^i - j_x^{i-1}}{j_x^i} \right| < \delta, \quad \text{for } i = i, \dots, i - T. \quad (13)$$

which is based on the momentum j_x calculated along the direction of the applied body force $B_x > 0$. This criterion can be understood as follows: simulation is terminated when the relative variation of momentum j_x between any pair of two consecutive iterations $i - 1$ and i does not exceed δ over T previous iterations. We stress the importance of satisfying the termination rule (13). Otherwise, the evaluation of M_1^i for a single iteration pair $(i - 1, i)$, even with a very small δ may terminate simulation too early. This can occur at the time of development of another momentum oscillation, followed by a slow but noticeable change in j_x . Our results are obtained for $\varepsilon = 10^{-9}$ and $T = 200$, while the fluid viscosity is $\nu = 0.5$ (or $\lambda^+ = 0.5$).

C. Discretization

The quality of mapping of analytical boundaries onto a discrete lattice is crucial to the accuracy of simulations in regular geometries such as periodic arrays of spheres. The main problem is that by default: i) each periodic cell contains just a few geometrical elements (spheres) to be discretized, and ii) the discrete lattice must contain an integer number of nodes along each dimension. In practice, substantial variation in lattice geometry can occur for a slight change of discretization resolution⁹. We note that this problem was partially addressed by Chun and Ladd, see Figure 8 in³⁶, who randomly moved the unit cell with spheres relative to the lattice and analyzed the corresponding error behavior. In the case of irregular sphere packings, this problem vanishes when the number of spheres becomes sufficiently large to sample the underlying lattice in different ways.

In this work, we apply the discretization approach that was suggested previously, see Figure 5 in⁹ and the supporting explanations. This approach exploits the periodicity property of a regular geometry, according to which we replicate a unit cell U times along each Cartesian direction and take the underlying lattice dimension L not evenly divisible by U . This leads to the non-integer lattice size per each unit cell L_{unit} , while having integer L for the whole lattice. In practice, the use of non-integer values of L_{unit} significantly reduces scatter in the simulated drag force (permeability), depicted in Figure 1. Extending the arguments above, the suggested discretization approach gives the best results when L and U have no common integer multipliers. For example, taking $L = 30$ and $U = 4$ ($L \bmod U \neq 0$) results in a drag value equivalent to the simulation setup with $L = 15$ and $U = 2$ because $L = 30$ and $U = 4$ have a common multiplier of 2; a better choice for $U = 4$ and $L \approx 30$ is $L = 29$ or $L = 31$.

Particular choice of U depends on the resolution and the porosity. From our experience of dealing with the BCC, FCC, SC packings of touching spheres, very low resolutions of 0.1–1 of lattice nodes per sphere diameter can require as many as $U \approx 10$ (resulting in U^3 unit cells), while for high resolutions of several hundred lattice nodes, $U = 2$ may be sufficient. It appears that the number of lattice voxels crossed by spheres *in different ways* is the key parameter that reduces scatter.

Our discretization approach produces the fully symmetric discrete lattices, i.e., each discretized geometry has reflection symmetry in all three Cartesian directions. In addition, we perform a slight variation of the sphere radius d_{sp} around its analytical value in order

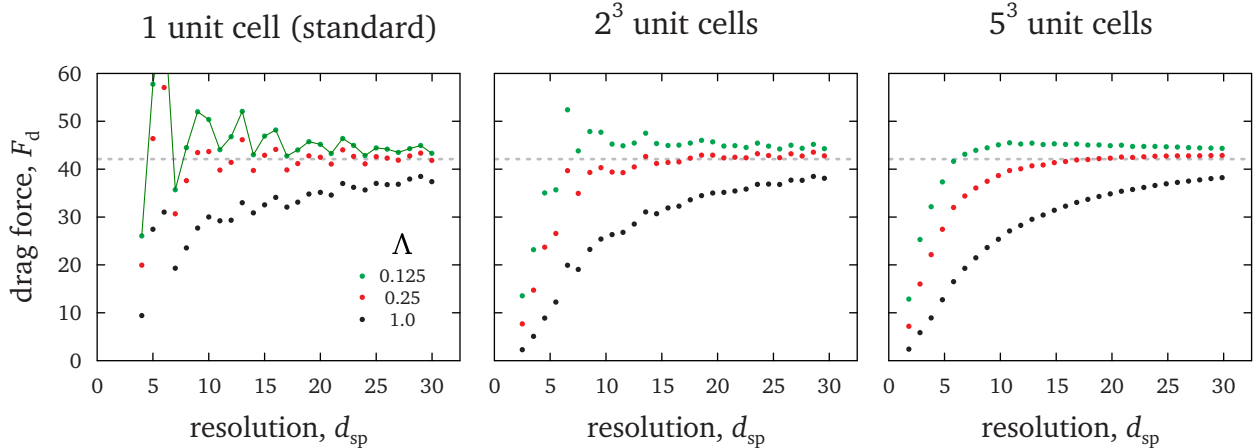


FIG. 1. Drag force vs. discretization resolution (in lattice units per sphere diameter) for simple cubic packing of touching spheres with $\varepsilon \approx 0.476$. Green, red, and black colors denote $\Lambda = 0.125$, 0.25, and 1.0, respectively. Reference drag value for this geometry is 42.1 (dashed line).

to obtain better agreement with the analytical and discrete porosities. The corresponding MATLAB scripts are available online³⁹.

D. Considered geometries and reference drag values

In this paper, we deal solely with regular packings of spheres that are commonly used to validate the numerical Stokes solutions^{9,15,30,36,40–42} and enable the in-depth comparisons of numerical simulations with previous works. This type of geometry can be approached analytically^{21–23}, but at the same time it captures the key features of flow in porous media and demonstrates more complex flow patterns, relative to open channels or pipes with circular or quadratic cross sections. We note that our approach is not limited to regular sphere packings and is applicable to the complex geometries, where the discretization resolution can be varied.

We consider three basic packing types (Figure 2) with unit cells of cubic shape and assume that they are filled with spheres of unit diameter. Face-centered cubic packing (FCC) has a unit cell edge $\sqrt{2}$ long, and is composed of 14 spheres: 6 are located in the centers of each face while 8 spheres are in the corners of the FCC unit cell. Body-centered cubic packing (BCC) has one sphere in the cell center and 8 in the corners and its edge is $2\sqrt{3}$ long. Simple cubic packing (SC) has unit edge length and a single sphere in the cell center. For all three

geometries, only parts of spheres that are inside of the corresponding unit cell are considered in flow simulations.

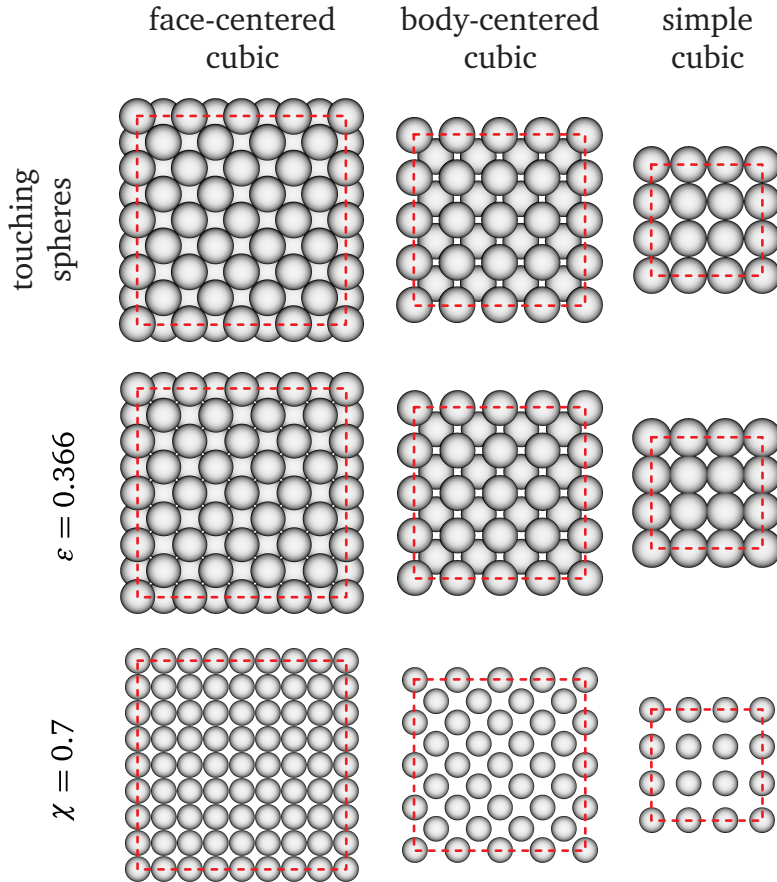


FIG. 2. Three packing types used in the simulations with unit cells replicated 4 times along each direction; the actual simulation domain is indicated with the red dashed lines. The middle row shows packings of fixed porosity ($\varepsilon = 0.366$) while the top and bottom rows depict touching and diluted packings, respectively.

In this study, we deal with accuracies of 10^{-3} or better in estimating drag force values. Special attention is given to the reference drag values because they should be trusted with accuracy of at least 10^{-4} . A careful examination of the previous non-LBM approaches for estimating drag in packings of the *touching* SC, BCC, and FCC spheres reveals disagreement between the studies by Zick and Homsy²², Sangani and Acrivos²¹, and Larson and Higdon²³ (see Table 5 in⁹). Therefore, for touching spheres we took drag values obtained from the high-resolution LBM simulations with the “parabolic” multi-reflection (MCLI) boundary condition. For the MCLI boundary condition, i) there is almost no dependency on Λ and ii)

	0.26	0.32	0.366	0.48	$\chi = 0.7$	0.784
FCC	432.0		146.5		9.7165	7.7576
BCC		162.8	114.4		8.5631	7.7388
SC			<u>84.85</u>	42.10	6.0042	7.4432

TABLE I. Reference drag values used in this work; packing types and porosities are given in the left column and top row, respectively. The value of $\chi = 0.7$ is the diameter scaling factor, which equals to 1.0 when spheres are touching. The factor χ is related to porosity as $\varepsilon = 1 - \chi^3(1 - \varepsilon^*)$ with ε^* denoting the porosity of a packing with touching spheres. Porosity values in **bold** are approximate and calculated as $\varepsilon_{\text{fcc}}^* = 1 - \pi/\sqrt{18} \approx 0.26$, $\varepsilon_{\text{bcc}}^* = 1 - \pi\sqrt{3}/8 \approx 0.32$, and $\varepsilon_{\text{sc}}^* = 1 - \pi/6 \approx 0.48$. Drag values in normal font are taken from the LBM/MCLI simulations⁹ while **bold** values are from the 30-term series expansion by Sangani²¹. The underlined drag value for the SC packing with the overlapping spheres and porosity of 0.366 is estimated from the extrapolation approach presented in this work with $d_{\text{sp}}^{\text{max}} \approx 429$ und $U = 3$.

the fast convergence rates of -3 or -4 provide the practically resolution-independent values of drag at high resolutions, with > 100 lattice nodes per sphere diameter.

Reducing sphere diameters with the contraction factor $\chi < 1$ increases the distance between sphere surfaces and results in better agreement among the published studies^{21–23}. Specifically, at the accuracy of at least 10^{-4} , the literature drag values become identical when $\chi \approx 0.7$ or less. Sangani and Acrivos²¹ provided a series expansion for the estimation of drag in FCC, BCC, and SC packings, which we adopt here to complement our study with the accurate drag force values in regular packings of high porosity. The corresponding values for the three regular packing types are listed in Table I.

The set of reference drag values for the touching and diluted regular packings is extended to the porosity of 0.366. For this porosity, there are solutions for BCC and FCC geometries available from Khirevich et al.⁹. These solutions were obtained at high-resolutions using LBM with the “parabolic” multi-reflection boundary schemes (MCLI)¹⁴. We also support this porosity with the SC geometry of overlapping spheres. We estimate its drag force with the approach presented in this paper.

III. GENERAL BEHAVIOR OF NUMERICAL ERROR

The two-relaxation-times collision operator controls the steady-state drag force solely through Λ . The Λ -dependency of the numerical solutions obtained with the bounce-back scheme in three regular packings is demonstrated in Figure 3. As mentioned previously⁹,

- Λ has the strongest impact on numerical error at low resolutions;
- error is non-monotonic with resolution increase, and it can significantly over- or underestimate true solution depending on a particular value of Λ ; and
- error behavior is similar for random and regular geometries or different porosities meaning that it is related to the method itself rather than to particular type of porous media.

In Figure 3, we further extend the understanding of error behavior. The non-monotonic convergence in Figure 3a–c can be related to the interplay among different error contributions: away from solid boundaries the lattice Boltzmann method performs with second-order accuracy³² while the first order¹³ bounce-back boundary condition is applied at the boundary nodes. This suggests existence of *at least* two contributions to the total simulation error, with quadratic and linear behavior. (There is one more contribution, related to the voxel-wise integration of three-dimensional flow field when calculating integral quantities such as average flow rate, but we omit it here.) An important point is that these contributions can have different signs and therefore compensate each other. This idea was discussed earlier, for instance in relation to the simulations of hypersonic flows⁴³. Mutual compensation of error contributions can lead to the very slow *transient* convergence rates, such as $-0.2 \dots -0.4$. Very slow convergence can be seen in other studies with the standard choice of relaxation parameters equivalent to $\Lambda = 0.25$ ($\tau = 1$ in the BGK collision operator)^{30,40,41}.

The bulk and boundary error contributions could eliminate each other, resulting in zero total error, but this never happens over the continuously varying resolutions, because convergence rates of the two contributions are different. In Figure 3d we provide a simple expression, $A/d_{\text{sp}} + B/d_{\text{sp}}^2$, which captures most of the error behavior obtained from the simulations. In fact, Λ can be seen as a parameter controlling the relative impact and sign of each error contribution.

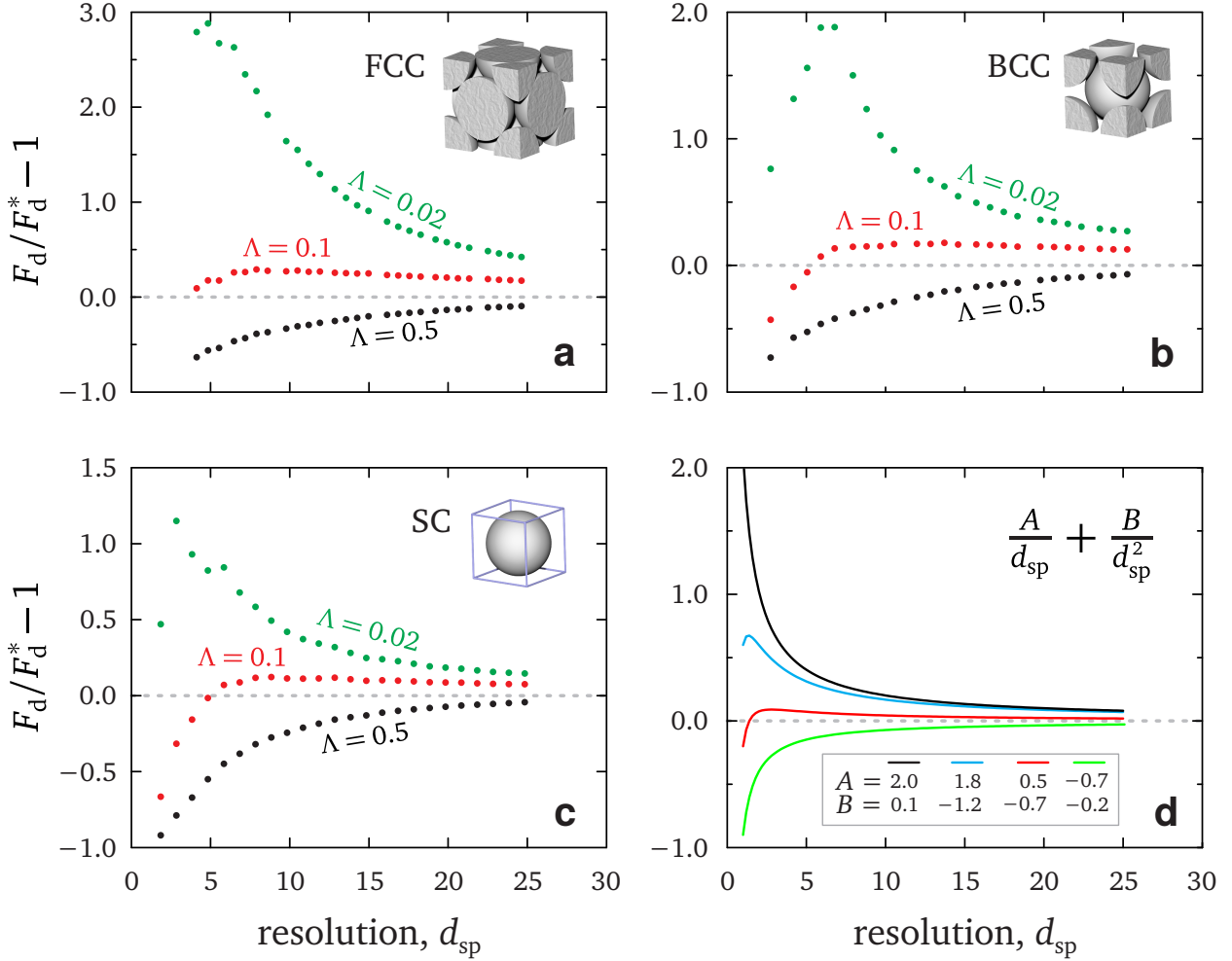


FIG. 3. a–c: Relative drag force error as a function of discretization resolution for FCC, BCC, SC packings of touching spheres; the dependencies are shown for three Λ values. d: a simple model that mimics variation of the quadratic and linear error convergence rates with resolution; shown are four different combinations of model parameters A and B .

Figure 4 is a double logarithmic plot of the low and high porosity cases in order to analyze their convergence rates. Here we consider a) the diluted FCC and BCC packings as well as the condensed SC packing of overlapping spheres, all three with $\varepsilon = 0.366$; and b) the FCC, BCC, and SC packings diluted to $\varepsilon = 0.784$. For Λ we took 0.25 and smaller to exclude negative error values, because for any value of Λ the drag error becomes positive with increasing resolution, but for $\Lambda > 1$ very fine meshes are necessary to observe this transition⁹. Figure 4 demonstrates that

- at very low resolutions ($d_{sp} < 5$) and low values of Λ , different packing types can

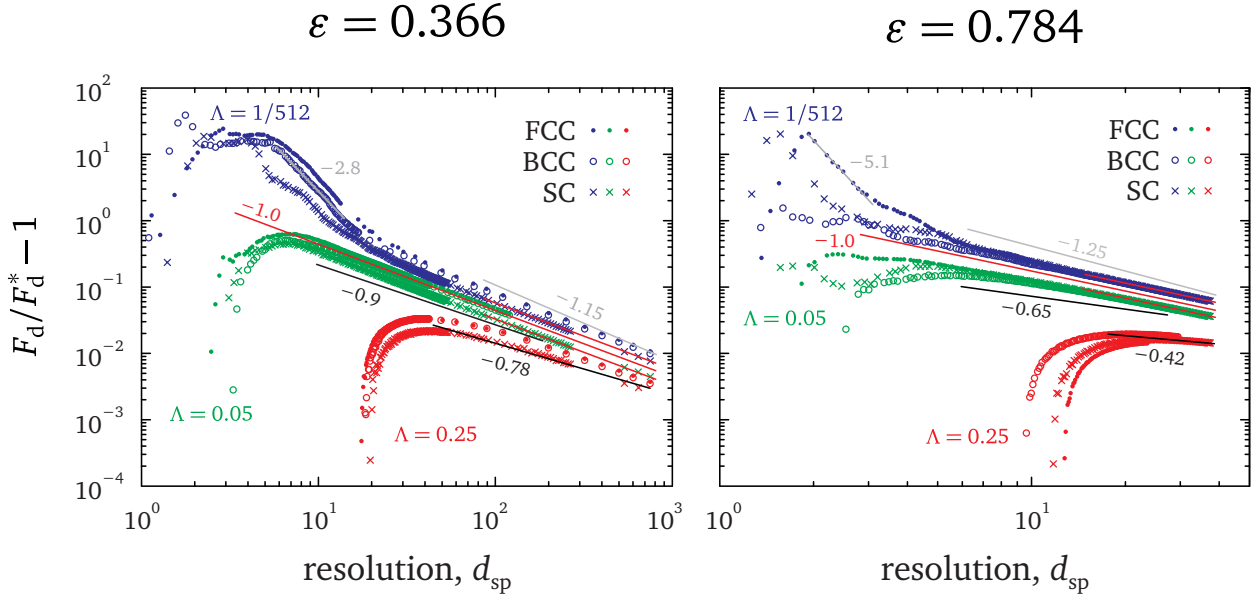


FIG. 4. Relative drag error vs. discretization resolution (in lattice nodes per sphere diameter). FCC, BCC, and SC packings of porosities $\varepsilon = 0.366$ and $\varepsilon = 0.784$ are considered. The SC packing with $\varepsilon = 0.366$ has overlapping spheres while the five other geometries are diluted regular packings. The results are obtained for $\Lambda = 1/512, 0.05, 0.25$. The lines indicate various convergence rates: red denotes the -1.0 rate, while gray is faster and black is slower than -1.0 .

demonstrate geometry-specific error behavior as well as very high convergence rates;

- for each porosity and at moderate or high resolutions, the errors weakly depend on a given geometry and are grouped for a particular value of Λ ; and
- depending on value of Λ , error approaches the -1 convergence rate from below (for $\Lambda = 0.25$ or higher) or from above ($\Lambda = 1/512$ or lower) for both porosities and all geometries.

The last statement extends some of the results of the previous work⁹: at infinitely high resolution the convergence rate will be -1.0 for any Λ (Figure 13 in⁹) and, therefore, extrapolating errors with different values of Λ to very high resolution ($> 10^4$) will not allow them to cross each other (Figure 14 in⁹).

The facts listed above suggest a simple extrapolation approach we discuss in the next section.

IV. EXTRAPOLATION APPROACH

The convergence rate of the slowest error contribution is -1.0 because of the bounce-back rule. It can be observed for any Λ with an increase of resolution. However, the particular choice of Λ defines the resolution region, where the error is dominated by the -1.0 contribution. It follows that the “magic parameter” Λ can be chosen so as to enforce transition to the -1.0 convergence rate at lower resolutions. After that any additional increase in resolution leads to linear error behavior and therefore can be predicted using a simple extrapolation. From our experience, the value of Λ close to 0.05 leads to the earliest transition to linear convergence for the considered packings and porosities. Therefore, we fix Λ to 0.05 for all extrapolation results.

Linear extrapolation requires at least two data points. Because of the residual discrete noise in the drag force values, even after improved discretization, we take six additional points (eight in total) to obtain each extrapolated value. There is no justification for this choice. We simply use additional points to make the extrapolation more robust. However, an important aspect is the distance between maximum $d_{\text{sp}}^{\text{max}}$ and minimum $d_{\text{sp}}^{\text{min}}$ resolutions in this set of points. For example, in the right panel of Figure 5 one can see oscillations of drag values around the extrapolation line. Such oscillations can impact the extrapolation result if $d_{\text{sp}}^{\text{max}}$ and $d_{\text{sp}}^{\text{min}}$ are too close (e.g., $d_{\text{sp}}^{\text{min}}/d_{\text{sp}}^{\text{max}} < 0.95$). Taking $d_{\text{sp}}^{\text{min}}$ too far away from $d_{\text{sp}}^{\text{max}}$ will place $d_{\text{sp}}^{\text{min}}$ in nonlinear region of the drag curve, see Figure 4, which too will negatively impact the extrapolation result. We found the ratio $d_{\text{sp}}^{\text{min}}/d_{\text{sp}}^{\text{max}} = 0.8$ to be a good choice, and use it to collect all extrapolated values. It worth mentioning that geometries with large amount of irregularly located objects are less impacted by discrete noise, and the statements above are less applicable.

In Figure 5, we present the extrapolation of drag force described above for the three basic packing types of touching spheres. In Figure 5 we also show the extrapolation with one of the standard choices of $\Lambda = 0.25$ resulting in $\tau = 1$ for BGK model. For instance, a similar approach was discussed in the study of Hoef et al. (Figures 2 and 3 in³⁴), in which the authors assumed quadratic ($1/d_{\text{sp}}^2$) error convergence. Use of the -2 extrapolation rate for the considered geometries and $\Lambda = 0.25$ slightly increases error in estimated drag values (data not shown). Dashed squares highlight the drag values for the highest employed resolutions using the standard simulation approach with $\Lambda = 0.25$ without any extrapolation procedures.

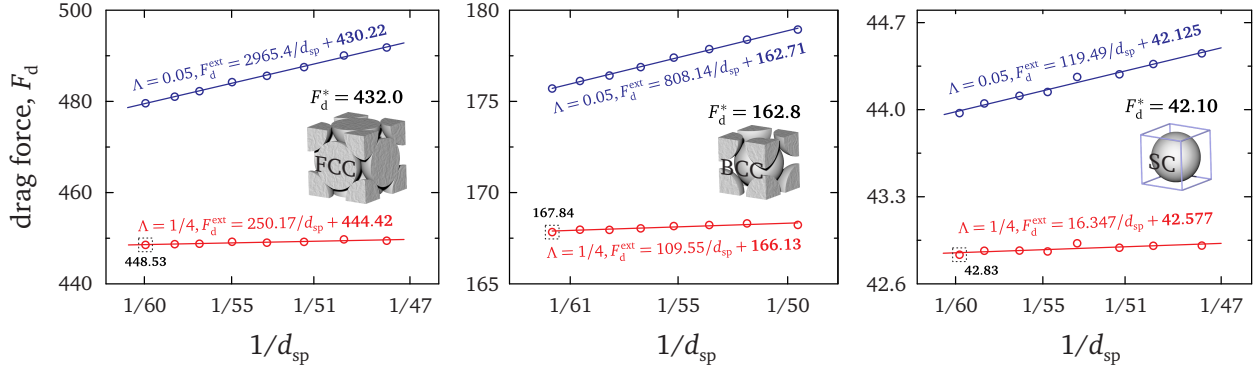


FIG. 5. Examples of extrapolation of drag values towards the infinitely-high discretization resolution assuming the solution convergence rate of -1 . The shown results are for the FCC, BCC, and SC packings of touching spheres. All extrapolation results in this study are obtained with $\Lambda = 0.05$.

To quantify accuracy and to compare the results of our numerical simulations with previous studies, we apply our extrapolation approach to the various packing types and porosities. Accurate reference values are taken from Table I. Figure 6 shows a strong increase of accuracy after applying the extrapolation procedure. The results for the touching spheres of low (FCC, BCC) and moderate (SC) porosities, as well as the porosity of 0.366, outperform standard bounce back approach by more than an order of magnitude.

For the high porosities with $\chi = 0.7$ that enforces $\varepsilon \approx 0.8$ for all packing types, the extrapolation approach performs comparably to the higher-order boundary schemes reported previously¹⁵. We note that in the work of Pan et al.¹⁵, the authors used two sets of relaxation parameters named “set A” and “set B”. We use the data from “set B” that corresponds to the two-relaxation-times collision operator we adopt here; $\tau = 0.6$ in their terms corresponds to $\Lambda = 3/16$ in this study. Slight tuning of Λ around 0.05 towards smaller values (see Figure 6) increases accuracy for the high-porosity case, but our primary focus is on the lower-porosity systems and therefore we stay with a single value of $\Lambda = 0.05$.

For the sake of completeness, we note that our attempts to take the large values of Λ (say, $\Lambda > 10$) and apply similar extrapolation approach to negative error region did not result in any meaningful outcomes. It appears that the error must cross zero first, become positive, and only then decrease to zero.

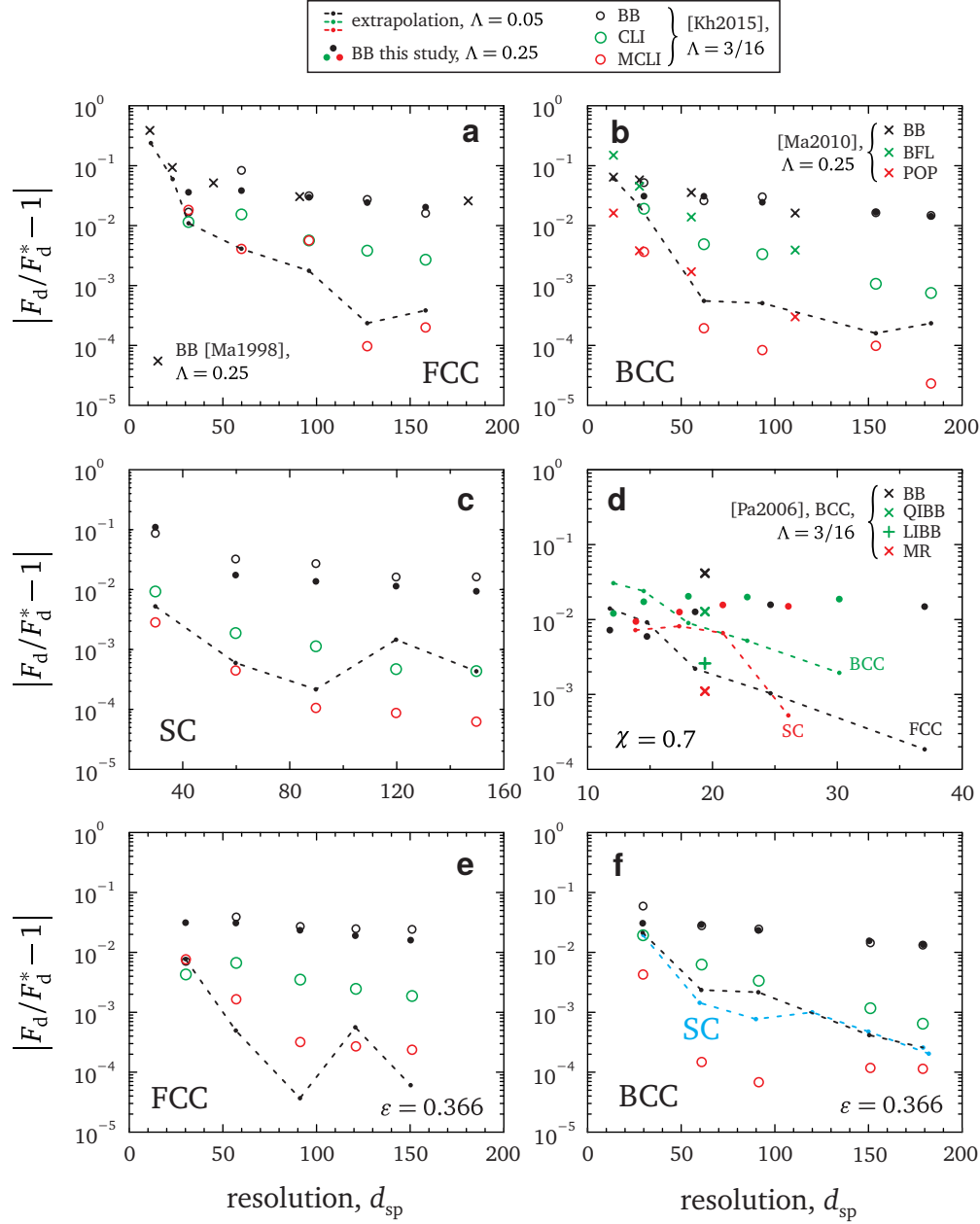


FIG. 6. Relative error in drag force for packings of touching (a–c) and diluted (d–f) spheres. a–c: Shown are the errors for the extrapolated drag force values (with $d_{sp} = d_{sp}^{\max}$) and the data taken from other studies: Tables 7, 8, 10 in Khirevich et al.⁹, as well as Table 1³⁰ and Table II⁴⁰ in Maier et al. Panel d) depicts errors for the diluted FCC, BCC, SC arrays with the diameter contraction factor of $\chi = 0.7$. The extrapolated values are compared with the results of Pan et al.¹⁵ for the BCC packing. CLI, MCLI, BFL, POP, QIBB, LIBB, MR refer to the higher-order boundary schemes. e,f) Error values for the FCC, BCC, SC packings with $\epsilon = 0.366$.

V. CONCLUSIONS AND OUTLOOK

In this paper, we have analyzed numerical error of the LBM bounce-back approximation of incompressible fluid flow and suggested a simple model for the simulation error. Our approach is based on the existence of at least two error contributions with the linear and quadratic decay rates of *different* signs. These error contributions amplify or compensate each other and, therefore, lead to the very fast (-3 or faster) or slow (slower than -0.5) *transient* convergence rates. All of these rates approach the -1 convergence rate sooner or later. This situation is not limited to LBM and also occurs in classic numerical approaches such as finite difference method – see error behavior in Figure 3 of Manwart et al.⁴¹ as an example.

The choice of $\Lambda = 0.05$ allowed to observe the -1 behavior at lower resolutions (of about 20 lattice nodes per sphere diameter for $\varepsilon = 0.366$, see Figure 4) and perform a linear extrapolation of drag values. The extrapolation results reduced the typical LBM/BB error by tens of times at medium resolutions (40 nodes and higher, Figure 6) and allowed to achieve accuracy of the high-order CLI and MCLI schemes. We note that there are no difficulties with programming the high-order boundary schemes for simple geometries while developing a serial program implementation of LBM. However, programming complexity increases for parallel applications and when dealing with obstacles distributed irregularly in space (for instance, see subsection 5.1 in³⁰). From this point of view, the suggested extrapolation approach can be seen as an alternative for improving simulation accuracy in some cases without modifying flow solver.

An extrapolated average velocity value does not provide accurate three-dimensional flow fields, but its knowledge can be used, for example, in simulations of hydrodynamic dispersion^{24,44}. Our preliminary studies suggest that using the extrapolated value of average velocity to calculate Péclet number improves accuracy of simulations of hydrodynamic dispersion with random-walk particle tracking method²⁴. This improvement can be attributed to the fact that variation of Λ moves the location of the zero-velocity boundary in a systematic way within the simulated geometry. A similar improvement can be obtained after scaling the Stokes flow velocity components with their accurate average value obtained from extrapolation.

The approach presented here requires variable resolutions of discretization of the pore space,

which is not always possible. Micro-CT images that often provide pore space geometry are usually limited to a single resolution. However, we see this study as a necessary step towards selecting optimal relaxation parameters in the pore-scale lattice-Boltzmann simulations.

ACKNOWLEDGMENTS

We are grateful for allocation of computational resources by the Supercomputing Laboratory at King Abdullah University of Science & Technology (KAUST) in Thuwal, Saudi Arabia.

REFERENCES

- ¹B. Ferréol and D. H. Rothman, “Lattice-Boltzmann simulations of flow through Fontainebleau sandstone,” *Transport in Porous Media* **20**, 3–20 (1995).
- ²G. Jin, T. W. Patzek, and D. Silin, “SPE 90084-MS: Direct Prediction of the Absolute Permeability of Unconsolidated and Consolidated Reservoir Rock,” in *SPE Annual Technical Conference and Exhibition* (SPE, Houston, TX, 2004).
- ³T. Ramstad, N. Idowu, C. Nardi, and P.-E. Øren, “Relative permeability calculations from two-phase flow simulations directly on digital images of porous rocks,” *Transport in Porous Media* **94**, 487–504 (2012).
- ⁴G. Jin, T. W. Patzek, and D. B. Silin, “Modeling the impact of rock formation history on the evolution of absolute permeability,” *Journal of Petroleum Science and Engineering* **100**, 153 – 161 (2012).
- ⁵D. B. Silin, G. Jin, and T. W. Patzek, “Robust determination of the pore-space morphology in sedimentary rocks,” *Journal of Petroleum Technology* **May**, 69 – 70 (2004).
- ⁶D. B. Silin and T. Patzek, “Pore space morphology analysis using maximal inscribed spheres,” *Physica A* **371**, 336 – 360 (2006).
- ⁷D. Silin, L. Tomutsa, S. M. Benson, and T. W. Patzek, “Microtomography and pore-scale modeling of two-phase fluid distribution,” *Transport in Porous Media* **86**, 495–515 (2011).
- ⁸E. Jettestuen, J. O. Helland, and M. Prodanović, “A level set method for simulating capillary-controlled displacements at the pore scale with

- nonzero contact angles,” *Water Resources Research* **49**, 4645–4661 (2013), <https://agupubs.onlinelibrary.wiley.com/doi/pdf/10.1002/wrcr.20334>.
- ⁹S. Khirevich, I. Ginzburg, and U. Tallarek, “Coarse- and fine-grid numerical behavior of MRT/TRT Lattice-Boltzmann schemes in regular and random sphere packings,” *J. Comp. Phys.* **281**, 708–742 (2015).
- ¹⁰P. L. Bhatnagar, E. P. Gross, and M. Krook, “A model for collision processes in gases. I. Small amplitude processes in charged and neutral one-component systems,” *Phys. Rev.* **22**, 511–525 (1954).
- ¹¹Y. Qian, D. d’Humières, and P. Lallemand, “Lattice BGK models for Navier-Stokes equation,” *Europhys. Lett.* **17**, 479–484 (1992).
- ¹²H. Chen, S. Chen, and W. H. Matthaeus, *Phys. Rev. A* **45**, R5339–R5342 (1992).
- ¹³I. Ginzbourg and P. M. Adler, “Boundary flow condition analysis for the three-dimensional lattice Boltzmann model,” *J. Phys. II* **4**, 191–214 (1994).
- ¹⁴I. Ginzburg and D. d’Humières, “Multireflection boundary conditions for lattice Boltzmann models,” *Phys. Rev. E* **68**, 066614 (2003).
- ¹⁵C. Pan, L.-S. Luo, and C. T. Miller, “An evaluation of lattice Boltzmann schemes for porous medium flow simulation,” *Comput. Fluids* **35**, 898–909 (2006).
- ¹⁶d’Humières, “Generalized lattice Boltzmann equations Rarefied Gas Dynamics: Theory and Simulations,” *Prog. Astronaut. Aeronaut.* **159**, 450–458 (1992).
- ¹⁷I. Ginzburg, F. Verhaeghe, and D. d’Humières, “Two-relaxation-time lattice Boltzmann scheme: About parametrization, velocity, pressure and mixed boundary conditions,” *Commun. Comput. Phys.* **3**, 427–478 (2008).
- ¹⁸I. Ginzburg, “Equilibrium-type and link-type lattice Boltzmann models for generic advection and anisotropic-dispersion equation,” *Adv. Wat. Res.* **28**, 1171–1195 (2005).
- ¹⁹D. d’Humières and I. Ginzburg, “Viscosity independent numerical errors for lattice Boltzmann models: From recurrence equations to “magic” collision numbers,” *Comp. Math. Appl.* **58**, 823840 (2009).
- ²⁰L. Talon, D. Bauer, S. Youssef, H. Auradou, and I. Ginzburg, “Equilibrium-type and link-type lattice Boltzmann models for generic advection and anisotropic-dispersion equation,” *Adv. Wat. Res.* **28**, 1171–1195 (2005).
- ²¹A. S. Sangani and A. Acrivos, “Slow flow through a periodic array of spheres,” *Int. J. Multiphase Flow* **8**, 343–360 (1982).

- ²²A. A. Zick and G. M. Homsy, “Stokes flow through periodic arrays of spheres,” *J. Fluid Mech.* **115**, 13–26 (1982).
- ²³R. E. Larson and J. J. L. Higdon, “A periodic grain consolidation model of porous media,” *Phys. Fluids* **38**, 38–46 (1989).
- ²⁴S. Khirevich, A. Daneyko, A. Höltzel, A. Seidel-Morgenstern, and U. Tallarek, “Statistical analysis of packed beds, the origin of short-range disorder, and its impact on eddy dispersion,” *J. Chromatogr. A* **1217**, 4713–4722 (2010).
- ²⁵T. Atmakidis and E. Y. Kenig, “Numerical Analysis of Residence Time Distribution in Packed Bed Reactors with Irregular Particle Arrangements,” *Chem. Prod. Process Model.* **10**, 17–26 (2015).
- ²⁶X. Frank and P. Perré, “Droplet spreading on a porous surface: A lattice Boltzmann study,” *Phys. Fluids* **24**, 042101 (2012).
- ²⁷M. Sbragaglia and S. Succi, “Analytical calculation of slip flow in lattice Boltzmann models with kinetic boundary conditions,” *Phys. Fluids* **17**, 093602 (2005).
- ²⁸M. A. A. Spaid and J. Frederick R. Phelan, “Lattice Boltzmann methods for modeling microscale flow in fibrous porous media,” *Phys. Fluids* **9**, 2468–2474 (1997).
- ²⁹D. Maggiolo, F. Picano, and M. Guarnieri, “Flow and dispersion in anisotropic porous media: A lattice-Boltzmann study,” *Phys. Fluids* **28**, 102001 (2016).
- ³⁰R. S. Maier and R. S. Bernard, “Lattice-Boltzmann accuracy in pore-scale flow simulation,” *J. Comp. Phys.* **229**, 233–255 (2010).
- ³¹M. Bouzidi, M. Firdaouss, and P. Lallemand, “Momentum transfer of a Boltzmann-lattice fluid with boundaries,” *Phys. Fluids* **13**, 3452–3459 (2001).
- ³²M. Junk and Z. Yang, “Convergence of lattice Boltzmann methods for Stokes flows in periodic and bounded domains,” *Comp. Math. Appl.* **55**, 1481–1491 (2008).
- ³³A. J. C. Ladd, “Numerical simulations of particulate suspensions via a discretized Boltzmann equation. Part 2. Numerical results,” *J. Fluid Mech.* **271**, 311–339 (1994).
- ³⁴M. A. van der Hoef, R. Beetstra, and J. A. M. Kuipers, “Lattice-Boltzmann simulations of low-Reynolds-number flow past mono- and bidisperse arrays of spheres: results for the permeability and drag force,” *J. Fluid Mech.* **528**, 233–254 (2005).
- ³⁵Y. Chen, J. R. Third, and C. R. Müller, “A drag force correlation for approximately cubic particles constructed from identical spheres,” *Chem. Eng. Sci.* **123**, 146–154 (2015).
- ³⁶B. Chun and A. J. C. Ladd, “Interpolated boundary condition for lattice Boltzmann

- simulations of flows in narrow gaps,” *Phys. Rev. E* **75**, 066705 (2007).
- ³⁷E. Fattahi, C. Waluga, B. Wohlmuth, U. Rde, M. Manhart, and R. Helmig, “Lattice Boltzmann methods in porous media simulations: From laminar to turbulent flow,” *Comput. Fluids* **140**, 247–259 (2016).
- ³⁸G. Silva and V. Semiao, “Consistent lattice Boltzmann modeling of low-speed isothermal flows at finite Knudsen numbers in slip-flow regime: Application to plane boundaries,” *Phys. Rev. E* **96**, 013311 (2017).
- ³⁹S. Khirevich, “MATLAB scripts for discretization of regular sphere packings,” <http://www.khirevich.com/lbm>, accessed: 15-08-2017.
- ⁴⁰R. S. Maier, D. M. Kroll, Y. E. Kutsovsky, H. T. Davis, and R. S. Bernard, “Simulation of flow through bead packs using the lattice Boltzmann method,” *Phys. Fluids* **10**, 60–74 (1998).
- ⁴¹C. Manwart, U. Aaltosalmi, A. Koponen, R. Hilfer, and J. Timonen, “Lattice-Boltzmann and finite-difference simulations for the permeability for three-dimensional porous media,” *Phys. Rev. E* **66**, 016702 (2002).
- ⁴²C. Chukwudozie and M. Tyagi, “Pore Scale Inertial Flow Simulations in 3-D Smooth and Rough Sphere Packs using lattice Boltzmann Method,” *Chem. Eng. Sci.* **59**, 4858–4870 (2013).
- ⁴³C. J. Roy, “Grid convergence error analysis for mixed-order numerical schemes,” *AIAA J.* **41**, 595–604 (2003).
- ⁴⁴R. S. Maier, D. M. Kroll, R. S. Bernard, S. E. Howington, J. F. Peters, and H. T. Davis, “Pore-scale simulation of dispersion,” *Phys. Fluids* **12**, 2065–2079 (2000).